

# Comparative Molecular Field Analysis of the Antitumor Activity of 9H-Thioxanthen-9-one Derivatives against Pancreatic Ductal Carcinoma 03

Jerome P. Horwitz,<sup>†\*</sup> Irina Massova,<sup>†</sup> Thomas E. Wiese,<sup>‡</sup> Brent H. Besler,<sup>§</sup> and Thomas H. Corbett<sup>†</sup>

Division of Hematology/Oncology, Department of Internal Medicine, and Department of Biochemistry, Wayne State University School of Medicine, and Department of Chemistry, Wayne State University, Detroit, Michigan 48201

Received November 12, 1993<sup>\*</sup>

The present study establishes correlations of *in vivo* growth inhibition of a solid tumor, pancreatic ductal adenocarcinoma (Panc 03), of mice with the steric and electrostatic fields and the hydrophobic parameter  $\log P$  of a series (32) of 1-[[2-(dialkylamino)alkyl]amino]-9H-thioxanthen-9-ones by the 3D-QSAR method comparative molecular field analysis (CoMFA). The template molecular model was hycanthonone methanesulfonate (19), the structure of which had been established previously by X-ray crystallography. The hycanthonone base is protonated at the terminal nitrogen N(2), and an intramolecular hydrogen bond is present between the proximal nitrogen N(1) and carbonyl oxygen O(1) atoms. Crystallographic data also indicate a planar arrangement of bonds around N(1). However, the molecular geometry of 19, optimized by semiempirical molecular orbital methods (PM3, MNDO, AM1), showed the expected trigonal-pyramidal configuration for N(1). A comparison of MO and *ab initio* methods applied to a model compound, 1-amino-9H-thioxanthen-9-one, led to the selection of PM3 as the method for full geometry optimization of first the cationic and then the neutral forms of 1-32, whereas AM1 provided atomic charges for these same structures save those incorporating a sulfonamide moiety (5, 7, 20, 25, 26, 29, 31, and 32). Acceptable values for the latter were obtained from *ab initio* calculations. Structures were aligned by minimizing root-mean-square (rms) differences in the fitting of structures to 19 using the FIT option of SYBYL. An alternative strategy of alignment, steric and electrostatic alignment (SEAL), was invoked to provide a comparison of statistical data generated with the rms alignment. The rms-fit alignment of structures produced slightly better cross-validated and conventional  $r^2$  values than those generated with the SEAL method. In addition, the rms-fit data indicate that a shift in the lattice of one-half of its spacing has a much smaller effect on the CoMFA data for a lattice of 1 Å than one of 2 Å. Inclusion of  $\log P$  in a CoMFA of the neutral structures effected a small (ca. 8-10%) but significant improvement in cross-validated  $r^2$  values. The relative contributions of the hydrophobic effects and the steric and electrostatic fields to the conventional  $r^2$  values were 16%, 42%, and 42%, respectively. By contrast, incorporation of frontier molecular orbital (HOMO and LUMO) energies or their gaps in the PLS analyses failed to enhance correlation coefficients derived for either the charged or uncharged compounds. Graphical results of the non-cross-validated CoMFA studies of the cationic structures are shown in the form of three-dimensional coefficient contour maps that delineate the steric and electrostatic features of the model. Figure 4 presents a view of the major steric fractions of the CoMFA contour map for an active (5) and inactive (6) analogue. Maps of the electrostatic field (Figure 5) indicate areas where positive or negative interactions favor tumor-growth inhibition. The present findings indicate, in accord with the rationale for CoMFA, that the interactions, which seem most appropriate for describing the anticancer activities of the 9H-thioxanthen-9-one derivatives, are noncovalent.

## Introduction

Several years ago, Baguley and co-workers deduced *in vivo* quantitative structure-activity relationships (QSAR) for a series of amsacrine analogues (9-substituted acridine derivatives) which provided a correlation of anticancer drug effects against a metastatic lung carcinoma model (3LL Lewis).<sup>1</sup> More recently, Schnur et al. described the synthesis and QSAR of a series of guanidinothiazolecarboxamides found to enhance the survival of mice bearing micrometastatic disease of 3LL.<sup>2</sup> These reports are of importance for additional reasons which include the fact that prior QSAR of anticancer drugs are, first of all, few in number and limited, essentially, to murine leukemia models. Moreover, cytotoxic anticancer drugs, which have

emerged as a result of teting among the several leukemia models and then demonstrated clinical utility in the treatment of various leukemias and lymphomas, have, in general, been rather ineffective against solid tumors, such as colon adenocarcinoma, non-small-cell lung cancers, and gastric and pancreatic carcinomas. These shortcomings have been ascribed to a screening strategy that, on the one hand, has been disease-focused but largely oriented against a single malignant disease, leukemia.

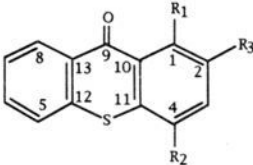
A disk-diffusion assay (see below), used routinely as a primary *in vitro* screen in our anticancer drug discovery program, identified a relatively wide series of 1-[[2-(dialkylamino)alkyl]amino]-9H-thioxanthen-9-ones that manifested solid tumor selectivity *vis-a-vis* antileukemia activity. These compounds had been developed originally as schistosomicidal agents,<sup>3,4</sup> but several were also tested *in vivo* subsequently as antitumor agents against P-388 (lymphocytic) leukemia.<sup>5</sup>

<sup>†</sup> Division of Hematology/Oncology, Department of Internal Medicine.

<sup>‡</sup> Department of Biochemistry.

<sup>§</sup> Department of Chemistry.

\* Abstract published in *Advance ACS Abstracts*, February 1, 1994.

**Table 1.** Structures and Activities of Some 9*H*-Thioxanthen-9-ones


compd	activity	R <sub>1</sub>	R <sub>2</sub>	R <sub>3</sub>
1	2	NHCH <sub>2</sub> CH <sub>2</sub> NEt <sub>2</sub>	CH=NPh	H
2	5	NHCH <sub>2</sub> CH <sub>2</sub> NEt <sub>2</sub>	CH <sub>2</sub> NHMe	H
3	2	NHCH <sub>2</sub> CH <sub>2</sub> NMe <sub>2</sub>	Me	H
4	5	NHCH <sub>2</sub> CH <sub>2</sub> NEt <sub>2</sub>	CH <sub>2</sub> NH <sub>2</sub>	H
5	5	NHCH <sub>2</sub> CH <sub>2</sub> NEt <sub>2</sub>	CH <sub>2</sub> NHSO <sub>2</sub> Me	H
6	-5	SCH <sub>2</sub> CH <sub>2</sub> NMe <sub>2</sub>	Me	H
7	3	NHCH <sub>2</sub> CH <sub>2</sub> NEt <sub>2</sub>	CH <sub>2</sub> NHSO <sub>2</sub> PhNH <sub>2</sub>	H
8	1	NHCH <sub>2</sub> CH <sub>2</sub> NEt <sub>2</sub>	CH <sub>2</sub> NMe <sub>2</sub>	H
9	3	NHCH <sub>2</sub> CH <sub>2</sub> NEt <sub>2</sub>	CH <sub>2</sub> SMe	H
10	0	NHCH <sub>2</sub> CH <sub>2</sub> NEt <sub>2</sub>	CH <sub>2</sub> OH	Me
11	2	NHCH <sub>2</sub> CH <sub>2</sub> NEt <sub>2</sub>	CH <sub>2</sub> OC(O)(CH <sub>2</sub> ) <sub>5</sub> Me	H
12	5	NHCH <sub>2</sub> CH <sub>2</sub> NEt <sub>2</sub>	CH <sub>2</sub> NHCHO	H
13	-5	N(Me)CH <sub>2</sub> CH <sub>2</sub> NEt <sub>2</sub>	CH <sub>2</sub> OH	H
14	1	NHCH <sub>2</sub> CH <sub>2</sub> NEt <sub>2</sub>	CH <sub>2</sub> OC(O)- <i>t</i> -Bu	H
15	-3	SCH <sub>2</sub> CH <sub>2</sub> NEt <sub>2</sub>	CH <sub>2</sub> OH	H
16	1	NHCH <sub>2</sub> CH <sub>2</sub> NEt <sub>2</sub>	CH <sub>2</sub> OMe	H
17	4	NHCH <sub>2</sub> CH <sub>2</sub> NEt <sub>2</sub>	C(O)NH <sub>2</sub>	H
18	0	NHCH <sub>2</sub> CH <sub>2</sub> NEt <sub>2</sub>	CH <sub>2</sub> OC(O)PhOMe	H
19	2	NHCH <sub>2</sub> CH <sub>2</sub> NEt <sub>2</sub>	CH <sub>2</sub> OH	H
20	4	NHCH <sub>2</sub> CH <sub>2</sub> NEt <sub>2</sub>	CH <sub>2</sub> N(Me)SO <sub>2</sub> Me	H
21	2	NHCH <sub>2</sub> CH <sub>2</sub> NEt <sub>2</sub>	CH <sub>2</sub> NHC(O)Ph	H
22	4	NHCH <sub>2</sub> CH <sub>2</sub> NEt <sub>2</sub>	CH <sub>2</sub> NHAc	H
23	4	NHCH <sub>2</sub> CH <sub>2</sub> NEt <sub>2</sub>	CH <sub>2</sub> N(CHO)Et	H
24	4	NHCH <sub>2</sub> CH <sub>2</sub> NEt <sub>2</sub>	CH <sub>2</sub> NHEt	H
25	3	NHCH <sub>2</sub> CH <sub>2</sub> NEt <sub>2</sub>	CH <sub>2</sub> NHSO <sub>2</sub> Ph	H
26	4	NHCH <sub>2</sub> CH <sub>2</sub> NMe <sub>2</sub>	CH <sub>2</sub> NHSO <sub>2</sub> Me	H
27	3	NHCH <sub>2</sub> CH <sub>2</sub> CH <sub>2</sub> NMe <sub>2</sub>	CH <sub>2</sub> NHMe	H
28	3	NHCH <sub>2</sub> CH <sub>2</sub> NMe <sub>2</sub>	CH <sub>2</sub> NHMe	H
29	5	NHCH <sub>2</sub> CH <sub>2</sub> CH <sub>2</sub> NMe <sub>2</sub>	CH <sub>2</sub> NHSO <sub>2</sub> Me	H
30	4	NHCH <sub>2</sub> CH <sub>2</sub> NMe <sub>2</sub>	CH <sub>2</sub> NH <sub>2</sub>	H
31	3	NHCH <sub>2</sub> CH <sub>2</sub> NEt <sub>2</sub>	CH <sub>2</sub> N(Me)SO <sub>2</sub> Et	H
32	4	NHCH <sub>2</sub> CH <sub>2</sub> NEt <sub>2</sub>	CH <sub>2</sub> N(Et)SO <sub>2</sub> Me	H

On the basis of the results of the disk-diffusion assays, 32 9*H*-thioxanthen-9-one derivatives were selected for evaluation against a solid tumor of mice. The present study establishes correlations of the *in vivo* target data with the steric and electrostatic fields and the hydrophobic parameter  $\log P$  of the 9*H*-thioxanthen-9-ones, bearing either a cationic or neutral (*N,N*-dialkylamino)alkyl side chain, by the method of comparative molecular field analysis (CoMFA). The need to apply CoMFA to the charged as well as neutral structures was recognized in the absence of evidence to indicate which of the two forms is the more important relative to the *in vivo* antitumor activities of this group of compounds.

### Biological Data

In an investigation of a relatively large number of agents, such as those comprising the series of 9*H*-thioxanthen-9-ones (Table 1, 1-32), it is virtually impossible to select a distinguishing criterion of biological activity which will provide the investigator with clear insight as to the potential worth of one analogue relative to the other members of the series. In many, perhaps the majority of cases, sufficient material is available for only a single evaluation, which further complicates and/or restricts the parameters of investigation. Indeed, it would be desirable to have, in hand, the breadth of activity of each agent against a large panel of tumors, complete with testing of multiple dose levels, route and schedule evaluations, advanced stage tumor treatments, and activities against multidrug resistant (MDR) tumors, etc. Because of cost constraints, criteria for resynthesis (and advancement to

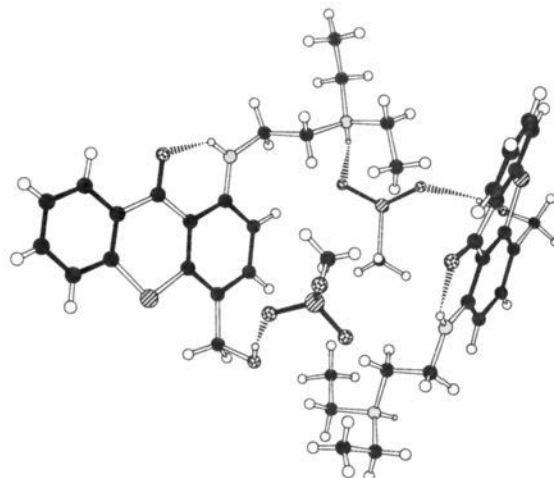


**Figure 1.** Crystal X-ray structure of hycanthone methanesulfonate (19), half unit-cell (see ref 11). Hydrogen bonds, in the form of dashed lines, have been added.

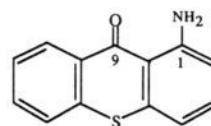


**Figure 2.** Model structure: 1-amino-9*H*-thioxanthen-9-one.

further evaluations) usually depend on multiple items of information derived from a single *in vivo* experiment. Corbett and co-workers have developed a soft agar disk-diffusion assay to identify agents that are selectively cytotoxic for solid tumors over leukemia L1210 and normal cells.<sup>6</sup> Furthermore, it has been demonstrated that if an agent has cellular selectivity for a solid tumor in the disk-diffusion assay (i.e., is more cytotoxic for the solid tumor than the leukemia), it is more likely to be active against many different types of solid tumors *in vivo*.<sup>6a,b,f</sup>

The 9*H*-thioxanthen-9-ones that displayed murine solid tumor selectivity in the disk-diffusion assay were evaluated against a transplantable solid tumor, pancreatic ductal adenocarcinoma (Panc 03), of mice.<sup>6a</sup> A numerical "activity" rating, based on a comparison of observed *in vivo* toxicity and tumor efficacy (see below), was assigned to each analogue. The reasons for the inclusion of the various arbitrary rating items, ranging from -1 to 4, as indicated below, are experience-based and, in general, self-evident. Obviously, greater antitumor activity is indicated by larger positive rating numbers. On the other hand, factors related to toxicity such as poor host tolerance to the drug, severe tissue-damaging properties, and efficacy restricted to only a single dose level or a very large dosage requirement are noted by subtractions. A well-tolerated agent with an excellent host recovery time is given a bonus point.

Toxicity: 1, acceptable toxicity (well-tolerated, rapid host recovery times); -1, active at one dose only; -1, violates 1100 mg/kg rule (excessively large dose requirement); -1, severe necrotizing activity; -1, poorly tolerated (slow host recovery, >7 days with the mice in poor physical condition).

Antitumor (Panc 03) efficacy (tumor/control (T/C)): 4, 0% T/C with 20% or cures; 3, 0-10% T/C; 2, 11-25% T/C; 1, 26-42% T/C.

### Computational Methods

A number of methods have been described to predict novel, biologically active compounds on the basis of previously synthesized and tested compounds.<sup>7</sup> Since its introduction in 1988, CoMFA<sup>8</sup> has produced excellent correlations with enzyme and

**Table 2.** Comparison of rms Deviations of Semiempirical MO and ab initio Methods for the Model Structure, based on the Crystallographic Data for 19

method	rms deviations	
	model structure	19
MNDO	0.399	0.896
AM1	0.183	1.335
PM3	0.157	0.967
ab initio <sup>a</sup>	0.141	

<sup>a</sup> GAUSSIAN92 settings HF 6-31G\*.**Table 3.** Comparison of ab initio and Semiempirical MO (MNDO, AM1, and PM3) Charges for the Model Compound

method	mean unsigned deviation of partial atomic charges
MNDO	0.231
AM1	0.183
PM3	0.216

**Table 4.** Partial Atomic Charges on N(1) and H(B) for the Model Compound

method	partial atomic charges	
	N(1)	H(B)
MNDO	-0.243	0.143
AM1	-0.353	0.243
PM3	0.046	0.092
ab initio	-0.959	0.449

receptor data<sup>9</sup> when utilized as a means to determine three-dimensional quantitative structure-activity relationships (3D-QSAR). The successful application of CoMFA to results from a whole-animal infectious disease model<sup>10</sup> prompted our interest in an attempt to apply the technique to in vivo antitumor data obtained with 1-32 (see Table 1).

The template molecular model was 1-[[2-(diethylamino)ethyl]-amino]-4-(hydroxymethyl)-9H-thioxanthen-9-one (19, hycanthone) methanesulfonate, the structure of which had been established previously by X-ray crystallography.<sup>11</sup> The latter served to generate, as well, the initial geometry of the corresponding neutral model. A computer representation of hycanthone (19, see Figure 1) was first constructed from the reported X-ray coordinates for the half unit-cell of this structure.<sup>11</sup> Crystallographic evidence indicates that the two outer rings of 19 are planar within 0.2° and these planes intersect along the central S(1)···C(9) line to form a slightly bent configuration with a dihedral angle of 167.7°. Additionally, the hycanthone base is protonated at the terminal nitrogen N(2), and an intramolecular hydrogen bond is present between the proximal nitrogen N(1) and carbonyl oxygen O(1) atoms. The existence of the latter results in a small torsion angle of -2° for atoms C(15)-N(1)-C(1)-C(2) and a planar arrangement of bonds (178.0°) around N(1), which may be due to the effect(s) of molecular packing and/or both inter(methanesulfonate salt) and intramolecular hydrogen bonds. By contrast, the molecular geometry of 19, optimized by the semiempirical molecular orbital methods PM3 and MNDO as well as AM1, using MOPAC (version 6.0),<sup>12</sup> indicated the expected trigonal-pyramidal configuration for N(1). However, the differences in the geometry of N(1), as indicated by MO methods vs crystallographic data, prompted the application of ab initio calculations to a model compound, 1-amino-9H-thioxanthen-9-one (Figure 2), the arbitrary selection of which, first of all, eliminates from consideration the intermolecular hydrogen bonds existing in the crystal and the distortions in the system that these bonds may induce. In addition, the model reduces the computational complexity of the problem that derives from the number of variables associated with the side chain of 19. The ab initio data were then compared both with the corresponding molecular geometries of the model compound, optimized by MO methods and, as well, with the X-ray data for 19. The comparison (see Results and Discussion) led to the selection of PM3 as the method for full geometry optimization of initially the cationic and then the neutral forms of 1-32, whereas AM1 provided atomic charges for these same structures save those incorporating a sulfonamide moiety (5, 7, 20, 25, 26, 29, 31,

**Table 5.** Comparison of Geometrical Features of 19 Selected from Crystallographic Data and Generated via Semiempirical MO Methods

method	dihedral angle between rms planes (deg)		hydrogen bond	
	to the rings A and C	C(1)-N(1)-C(15) and C(1)-N(1)-H(B)	distance between O(1) and H(B) (Å)	angle O(1)-H(B)-N(1) (deg)
	X-ray	167.57	177.98	1.851
MNDO	146.35	140.54	2.628	105.32
AM1	166.51	130.98	2.219	112.01
PM3	163.18	130.53	1.851	132.93

**Table 6.** Comparison of CoMFA Results Derived from Cationic Structures using Different Lattice Spacings and based on SEAL

$\alpha$	$1/\sqrt{\alpha}$ (Å)	2 Å		1 Å	
		cross-validated	conventional	cross-validated	conventional
0.20	2.24	0.536	0.951	0.614	0.958
0.25	2.00	0.541	0.958	0.616	0.959
0.30	1.83	0.556	0.963	0.618	0.959
0.40	1.58	0.553	0.964	0.623	0.964
0.50	1.41	0.552	0.963	0.628	0.967
0.60	1.29	0.556	0.963	0.628	0.968
0.70	1.20	0.558	0.962	0.629	0.969
0.80	1.12	0.561	0.962	0.632	0.969
0.90	1.05	0.564	0.962	0.634	0.969
1.00	1.00	0.568	0.962	0.636	0.970
1.10	0.95	0.569	0.962	0.636	0.970
1.20	0.91	0.570	0.962	0.636	0.970
1.30	0.88	0.569	0.962	0.636	0.970
1.50	0.82	0.567	0.963	0.633	0.971
1.70	0.77	0.559	0.964	0.632	0.971

and 32). Acceptable values for the latter were obtained from ab initio calculations.

Structures were aligned by minimizing root-mean-square (rms) differences in the fitting of four aromatic carbon atoms, C(10)-C(13), of each structure to the same atoms of the corresponding cationic and neutral forms of 19 using the FIT option of SYBYL, version 6.0.<sup>13</sup> An alternative strategy of alignment, steric and electrostatic alignment (SEAL),<sup>14</sup> which we employed in an earlier study,<sup>15</sup> was invoked to provide a comparison of statistical data generated with the rms alignment of only the cationic structures.

CoMFA was performed with the QSAR option of SYBYL. The requisite three-dimensional lattice, with 2-Å spacings in the  $x$ ,  $y$ , and  $z$  directions, generated automatically by the software, was utilized with both the SEAL and rms alignments. This grid region overlapped all entered molecules and extended beyond their volumes by at least 4 Å along all axes. The statistical findings were then compared to results obtained using both methods of alignment and a grid region of the same size but with spacings of 1 Å. Steric and electrostatic interactions at lattice intersections of both grids were generated with a probe atom that had the van der Waals properties of an  $sp^3$  carbon and a charge of 1.0.

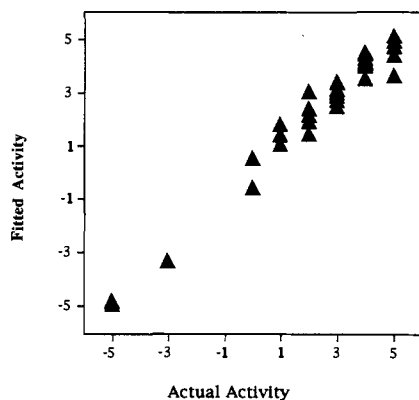
The linear expression of the CoMFA results was calculated with the partial least-squares (PLS) analysis algorithm in conjunction with the cross-validation procedure. The calculation provides (inter alia) a determination of the optimal number of components, i.e., that which yields the optimally predictive model as indicated by the highest correlation (predictive  $r^2$ ) value. PLS analysis of the descriptors with the same number of components but without cross-validation afforded conventional  $r^2$  values.

## Results and Discussion

Table 2 indicates that the ab initio approach predicts a geometry for the model structure with the smallest rms deviation from that based on crystallographic data for (cationic) 19. Of the semiempirical MO methods, PM3 generates a geometry for the model which most closely resembles that of the X-ray data. On the other hand, AM1 is the better electrostatic descriptor, as is evident from a comparison of the mean unsigned MOPAC charge deviations (Table 3) and of the partial atomic charges on

Table 7. Comparison of CoMFA Results with Different Spacings and Offsets of Lattice, based on rms Alignment

spacing (Å)	offset (Å)			steric and electrostatic fields only, cationic structures		steric and electrostatic fields only, neutral structures		steric and electrostatic fields and log <i>P</i> , neutral structures	
	<i>x</i>	<i>y</i>	<i>z</i>	cross-validated <i>r</i> <sup>2</sup>	conventional <i>r</i> <sup>2</sup>	cross-validated <i>r</i> <sup>2</sup>	conventional <i>r</i> <sup>2</sup>	cross-validated <i>r</i> <sup>2</sup>	conventional <i>r</i> <sup>2</sup>
	2	0.0	0.0	0.0	0.571	0.977	0.670	0.971	0.699
2	1.0	0.0	0.0	0.605	0.975	0.563	0.949	0.616	0.956
2	0.0	1.0	0.0	0.654	0.943	0.635	0.958	0.716	0.944
2	0.0	0.0	1.0	0.570	0.957	0.576	0.950	0.659	0.946
mean				0.600	0.963	0.611	0.957	0.673	0.951
1	0.0	0.0	0.0	0.647	0.968	0.603	0.963	0.653	0.950
1	1.0	0.0	0.0	0.640	0.968	0.635	0.973	0.671	0.955
1	0.0	1.0	0.0	0.629	0.964	0.586	0.968	0.654	0.953
1	0.0	0.0	1.0	0.643	0.967	0.633	0.968	0.675	0.951
mean				0.640	0.967	0.614	0.968	0.663	0.952

Figure 3. Actual vs fitted activities of 9*H*-thioxanthen-9-ones (1–32) against transplantable Panc 03 tumor of mice.

N(1) and H(B) shown in Table 4. In addition, partial atomic charges for structures 5, 7, 20, 25, 26, 29, 31, and 32, as noted above, include ab initio charges for a sulfonamide moiety.

Application of the three MO methods to the geometry optimization of 19 indicates (Table 2), in contrast to the results with the model, that MNDO produces the smallest rms deviation from the X-ray data. However, the suggestion may not be accurate in view of the fact that MNDO, in this particular application, gives rise to an exaggerated "butterfly-like" structure for the polycyclic system of 19. Coincidentally, MNDO leads to a geometry approximating that of the crystal structure. However, in the solid, a distortion of structure and a consequent rotation of the side chain are seen to occur due to intermolecular hydrogen bonding. The latter interaction is, obviously, excluded in the model.

The plane angles of the polycyclic system comprising 19, as predicted by both AM1 and PM3 but not by MNDO, are in reasonable agreement with the corresponding X-ray data (cf. Table 5). But all three semiempirical methods favor a pyramidal arrangement of bonds around N(1) rather than the planar structure indicated by crystallographic data. On the other hand, only PM3 reproduces the intramolecular O(1)–H(B) hydrogen-bond distance<sup>16</sup> and O(1)–H(B)–N(1) angle observed in the crystal (Table 5). These parameters are of importance not only with respect to the orientation of the pendant [(diethylamino)ethyl]amino chain but, very probably as well, in the presentation of the entire structure (19) to the ultimate but presently unknown receptor associated with antitumor activity.

A comparison of CoMFA-derived QSAR indicates, in accord with our previous results,<sup>15</sup> that with lattice spacings

of either 2 or 1 Å, the SEAL method gives *r*<sup>2</sup> values approaching those obtained with the rms fit but only with the alignment function parameter,  $1/\sqrt{\alpha}$ , of SEAL set at values  $\leq 1.0$  (Table 6). In addition, the data indicate, as noted previously,<sup>15</sup> that a shift in the lattice of one-half of its spacing has a much smaller effect on the CoMFA data for a lattice of 1 Å than one of 2 Å (Table 7). However, the smaller lattice spacing required a (40–60)-fold increase in computational time to obtain the data.

In the absence of pharmacokinetic information regarding the distribution of the 9*H*-thioxanthen-9-ones in biological fluids and tissues, it was of interest to determine whether or not differences would be observed in the partial least-squares analysis of cationic vis-a-vis and neutral structures. However, the QSAR failed to show a statistical difference among correlation coefficients generated with the two forms at lattice spacings of either 2 or 1 Å (Table 7). This is not surprising in view of the fact that CoMFA looks at differences, rather than absolute values, among field properties.<sup>17</sup>

A multiple regression analysis, performed on the 9*H*-thioxanthen-9-ones listed in Table 1, failed to show a significant correlation of the efficacy of these compounds as anticancer agents and the hydrophobicity factor log *P*, as specified by the atomic increments approach of Ghose and Crippen.<sup>18</sup>

$$\text{activity} = 5.991 - 1.266 \log P$$

$$n = 32 \quad r^2 = 0.247 \quad s = 2.314 \quad F_{1,30} = 9.818 \quad p = 0.004$$

Thus, log *P*, by itself, is a poor descriptor of activity. By contrast, inclusion of log *P* in a CoMFA of the neutral structures effected a small (ca. 8–10%) but significant improvement in cross-validated *r*<sup>2</sup> values. The relative contributions of the hydrophobic effects and the steric and electrostatic fields to the conventional *r*<sup>2</sup> values were 16%, 42%, and 42%, respectively. Despite the smaller contribution, log *P* is deemed important by virtue of its association with transport and distribution (pharmacokinetics) in biological fluids and tissues. Accordingly, the influence of this factor on the activities of drugs in whole animals must be considered. In this connection, Hansch has noted that the physicochemical parameter log *P* accounts for a number of hydrophobic interactions, which have relevance not only in the random walk of a ligand to a receptor but also to its receptor binding and metabolic modification.<sup>19</sup>

By contrast, incorporation of parameters such as frontier molecular orbital (HOMO and LUMO) energies or their gaps in the PLS analyses failed to enhance the correlation

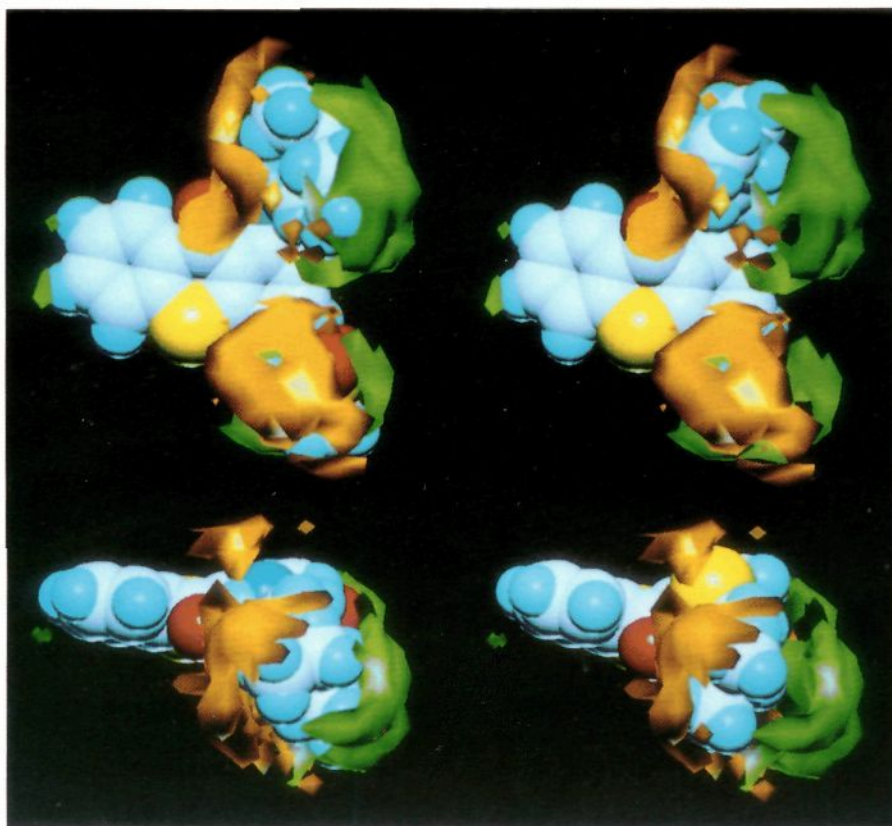


**Figure 4.** Orthogonal views of compounds 5 and 6 embedded in contour maps derived from the steric CoMFA model. Surrounding opaque surfaces represent the product of the standard deviation times the QSAR coefficient corresponding to values of  $\pm 0.009$  for green and orange areas, respectively.

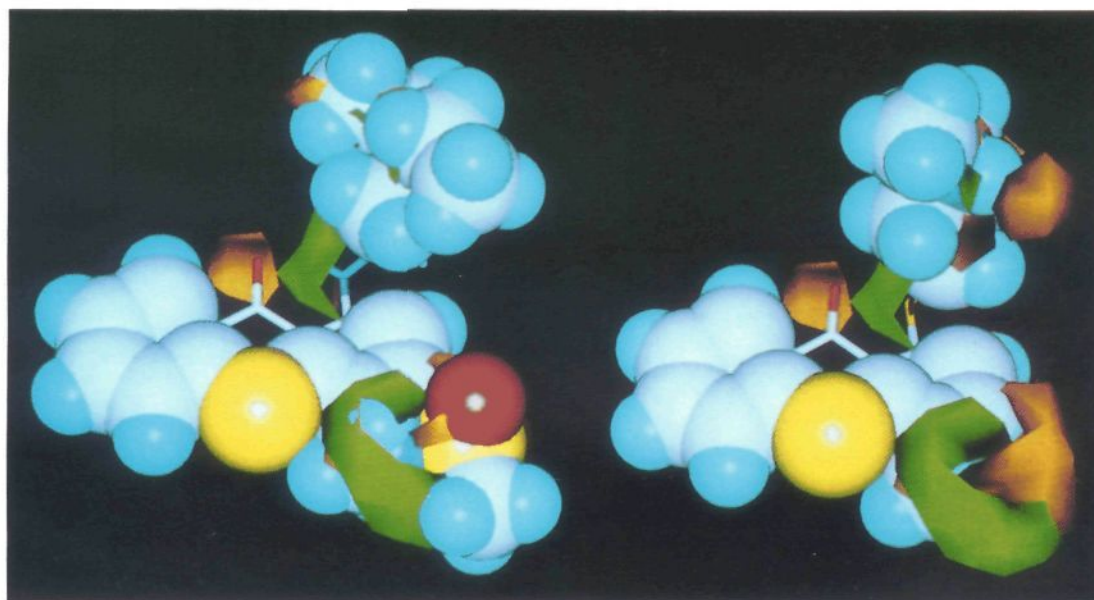


**Figure 5.** Front views of compounds 5 and 6 embedded in contour maps derived from the electrostatic CoMFA model. Surrounding green and orange opaque surfaces are as described in Figure 4.

coefficients derived for either the charged or uncharged compounds (data not shown). Thus, the QSAR provided no additional insights regarding the transition state leading to drug-receptor interactions.

The cross-validated  $r^2$  values (Table 6 and 7) indicate the considerable predictive capacity of the CoMFA-derived model as is evident in a plot (Figure 3) of actual vs fitted activities of 32 (cationic) compounds against Panc 03. Graphical results of the non-cross-validated CoMFA

studies of the cationic structures are shown in Figures 4 and 5 in the form of three-dimensional contour maps (based on Table 7; lattice spacing 1 Å, offset 0,  $r^2 = 0.968$ ) that delineate the steric and electrostatic features of the CoMFA model. Figure 4 presents a view of the steric contour map containing an active (right, 5) and inactive (left, 6) analogue, respectively. Surrounding green and orange surfaces represent regions where the product of the standard deviation times the QSAR coefficient cor-

responds to values of favorable (green, 0.009) and unfavorable (orange, -0.009) steric interaction. An increase in steric bulk in the green region and/or a decrease of the same in the orange area would enhance activity.

An intramolecular hydrogen bond between the proximal nitrogen N(1) and carbonyl oxygen O(1) atoms, a planar arrangement of bonds around N(1), and a small torsion angle for atoms C(15)-N(1)-C(1)-C(2), all indicated in the crystallographic data for **19**, lead to a configuration of the C(1)-exocyclic substituents in **5** which, overall, is within the green but outside the orange surfaces and, therefore, constitute a favorable arrangement for activity.

The virtually coplanar configuration of carbonyl oxygen O(1) and C(15)-N(1)-C(1)-C(2), evident in **5**, is not attainable in **6** with the loss of the intramolecular hydrogen bond on substitution of S for HN(1). The effect of substitution, coupled with a consequent change in the disposition of the (dimethylamino)ethyl group, leads to a geometry of the side chain in **6** which is unfavorable for activity. Indeed, the C(1)-exocyclic substituents are now seen to lie distal to the green surface and, instead, in rather close proximity to the orange surface wherein steric bulk is associated with reduced activity.

Figure 5 depicts structures **5** and **6**, embedded in contour maps derived from the electrostatic CoMFA model, and indicates areas where positive or negative interactions favor tumor-growth inhibition (same color-coded regions as in Figure 4). The positively (proximal H(B)) and negatively (carbonyl oxygen and N(1)) polarized participants in the intramolecular hydrogen bond in **5** (absent in **6**) lie adjacent to green and orange surfaces, respectively. Thus, the contour coefficient maps indicate that these dipole-dipole interactions in the 9*H*-thioxanthen-9-one analogues contribute to the inhibition of Panc 03 growth.

The meaning of the contour plots, as they relate in particular to the electrostatic charges that surround the CH<sub>2</sub>-X (X = OH and NH<sub>2</sub>, etc.) substituent attached at C(4), is not apparent. Thus, the relatively acidic hydrogen atom of, for example, -NHSO<sub>2</sub>CH<sub>3</sub> (**5** and as well the other amide derivatives), in contrast to that of the CH<sub>3</sub> group of **6**, is enveloped in a positive contour region. However, a hydrogen of the equally active primary and secondary amines, **4** and **2**, as well as that of the less active primary alcohol derivative, e.g., **19**, is in favorable electrostatic space. These ambivalent results indicate that the electrostatic interactions of the C(4) substituents (and presumably those that relate to the steric contour as well), though undoubtedly involved in determining the antitumor activities of **1-32**, play a less important role than those of the [(dialkylamino)alkyl]amino side chain in conjunction with the polycyclic structure.

The present findings indicate, in accord with the rationale for CoMFA,<sup>8</sup> that the interactions, which seem most appropriate for describing the anticancer activities of the 9*H*-thioxanthen-9-one derivatives, are noncovalent. Indeed, the results lend support to the utility of this 3D-QSAR approach to an in vivo study.<sup>9</sup>

**Acknowledgment.** All of the 9*H*-thioxanthen-9-ones used in this study were generously provided by the Sterling Winthrop Laboratories/Eastman Kodak Corporation. This investigation was supported in part by a Program Project Research Grant, CA 46560, from the National Cancer Institute.

## References

- (1) (a) Baguley, B. C.; Finlay, G. J. Derivatives of Amsacrine: Determinants Required for High Activity against Lewis Lung Carcinoma. *J. Natl. Cancer Inst.* 1988, 80, 195-199. (b) Atwell, G. J.; Baguley, B. C.; Finlay, G. J.; Rewcastle, G. W.; Denny, W. A. 3'-Methylamino Derivatives of Amsacrine with In Vivo Solid Tumor Activity. *J. Med. Chem.* 1986, 29, 1769-1776.
- (2) Schmur, R. C.; Gallaschun, R. J.; Singleton, D. H.; Grissom, M.; Sloan, D. E.; Goodwin, P.; McNiff, P. A.; Fliri, A. F. J.; Mangano, F. M.; Olson, T. H.; Pollack, V. A. Quantitative Structure-Activity Relationships of Antitumor Guanidinothiazolecarboxamides with a Survival Enhancement for Therapy in the 3LL Lewis Lung Carcinoma Model. *J. Med. Chem.* 1991, 34, 1975-1982.
- (3) Mauss, H. Basically Substituted Xanthane and Thioxanthane Derivatives; Miracil, a New Chemotherapeutic Agent. *Chem. Ber.* 1948, 81, 19-31.
- (4) Rosi, D.; Peruzzotti, G.; Dennis, E. W.; Berberian, D. A.; Freele, H.; Tullar, B. F.; Archer, S. Hycanthone, A New Active Metabolite of Lucanthone. *J. Med. Chem.* 1967, 10, 867-876.
- (5) Archer, S.; Pica-Mattocchia, L.; Cioli, D.; Seyed-Mozaffari, A.; Zayed, A.-H. Preparation and Antischistosomal and Antitumor Activity of Hycanthone and Some of its Congeners. Evidence for the Mode of Action of Hycanthone. *J. Med. Chem.* 1988, 31, 254-260.
- (6) (a) Corbett, T. H. A Selective Two-Tumor Soft Agar Assay for Drug Discovery. *Proc. Am. Assoc. Cancer Res.* 1984, 25, 325. (b) Corbett, T. H.; Wozniak, A.; Gerpheide, S.; Hanka, L. A.; Valeriote, F. A. Rodent Models in Experimental Chemotherapy. In *The Use of Rodent Tumors in Experimental Cancer Chemotherapy: Conclusions and Recommendations*; Kallman, R. F., Ed.; Pergamon Press: New York, 1987; Chapter 50, pp 233-247. (c) Corbett, T. H.; Wozniak, A.; Gerpheide, S.; Hanka, L. A. A Selective Two-Tumor Soft Agar Assay for Drug Discovery. In *In Vitro and In Vivo Models for Detection of New Antitumor Drugs*, Fourteenth International Congress of Chemotherapy, Tokyo, Japan; White, E., Ed.; University of Tokyo Press: Tokyo, 1987, pp 5-14. (d) Corbett, T. H.; Bissery, M.; Wozniak, A.; Plowman, J.; Polin, L.; Tapazoglou, E.; Dieckman, J.; Valeriote, F. Activity of Flavone Acetic Acid (NSC 34712) against Solid Tumors of Mice. *Invest. New Drugs* 1986, 4, 207-220. (e) LoRusso, P. M.; Polin, L.; Bissery, M. C.; Valeriote, F.; Plowman, J.; Corbett, T. H. Activity of Batracynin (NSC 320846) against Solid Tumors of Mice. *Invest. New Drugs* 1989, 6, 295-306. (f) LoRusso, P.; Wozniak, A. J.; Polin, L.; Capps, D.; Leopold, W. R.; Werbel, L. M.; Biernat, L.; Dan, M. E.; Corbett, T. H. Antitumor Efficacy of PD115934 (NSC 366140) against Solid Tumors of Mice. *Cancer Res.* 1990, 50, 4900-4905.
- (7) For a comprehensive list of literature references relevant to this topic, see: Klebe, G.; Abraham, U. On the Prediction of Binding Properties of Drug Molecules by Comparative Molecular Field Analysis. *J. Med. Chem.* 1993, 36, 70-80.
- (8) Cramer, R. D., III; Patterson, J. E.; Bunce, J. D. Comparative Molecular Field Analysis (CoMFA). 1. Effect of Shape on Binding of Steroids to Carrier Proteins. *J. Am. Chem. Soc.* 1988, 110, 5959-5967.
- (9) A recent summary of literature references to the application of CoMFA in the determination of three-dimensional quantitative structure-activity relationships is contained in: McFarland, J. W. Comparative Molecular Field Analysis of Anticoccidial Triazines. *J. Med. Chem.* 1992, 35, 2543-2550.
- (10) See McFarland, J. W., ref 9.
- (11) Wei, C. S.; Einstein, J. R. The Structure of Hycanthone Methanesulfonate, [C<sub>20</sub>H<sub>24</sub>N<sub>2</sub>O<sub>2</sub>S][CH<sub>3</sub>SO<sub>3</sub>H]: An Antischistosomal Agent. *Acta Crystallogr.* 1978, B34, 205-212.
- (12) (a) Stewart, J. J. P. MOPAC: A General Molecular Orbital Package (Version 6.0). *Quantum Chemistry Program Exchange Catalogue (QCPE)* 1992, IV, 19-20. (b) Stewart, J. J. P. MOPAC: A Semiempirical Molecular Orbital Program. *J. Comput.-Aided Mol. Des.* 1990, 4, 1-105.
- (13) Tripos Associates, 1699 S. Hanley Rd, Suite 303, St. Louis, MO 63144.
- (14) Kearsley, S. K.; Smith, G. M. An Alternative Method for Alignment of Molecular Structures: Maximizing Electrostatic and Steric Overlap. *Tetrahedron Comput. Methodol.* 1990, 3, 615-633.
- (15) Horwitz, J. P.; Massova, I.; Wiese, T. E.; Wozniak, A. J.; Corbett, T. H.; Sebolt-Leopold, J. S.; Capps, D. B.; Leopold, W. R. Comparative Molecular Field Analysis of In Vitro Growth Inhibition of L1210 and HCT-8 Cells by Some Pyrazoloacridines. *J. Med. Chem.* 1993, 36, 3511-3516.
- (16) Among the principal drawbacks of MNDO is the fact that the hydrogen bond is virtually nonexistent. See ref 10b, p 43.
- (17) The authors are indebted to the reviewer for this suggestion.
- (18) Ghose, A. K.; Crippen, G. M. Atomic Physicochemical Parameters for Three-Dimensional Structure-Directed Quantitative Structure-Activity Relationships. 2. Modeling Dispersive and Hydrophobic Interactions. *J. Chem. Inf. Comput. Sci.* 1987, 27, 21-35.
- (19) Hansch, C. Quantitative Structure-Activity Relationships and the Unnamed Science. *Acc. Chem. Res.* 1993, 26, 147-153.